ELSEVIER

Contents lists available at ScienceDirect

Chemical Engineering Science

journal homepage: www.elsevier.com/locate/ces



Understanding the difference between 2D and 3D simulations: How can a 2D CFD model rationally predict gastric emptying?

Xin Zhang ^a, Xianchen Huang ^b, Xiao Dong Chen ^a, Jie Xiao ^{a,*}

- ^a School of Chemical and Environmental Engineering, College of Chemistry, Chemical Engineering and Materials Science, Soochow University, Suzhou, Jiangsu 215123, China
- b The Fourth Affiliated Hospital of Soochow University, Suzhou, Jiangsu 215123, China

ARTICLE INFO

Keywords: Gastric emptying Pyloric opening and closure Computational fluid dynamics (CFD) Surrogate model

ABSTRACT

Two-dimensional (2D) computational fluid dynamics (CFD) models have been conventionally adopted for simulating a wide range of fluid flow problems. It is especially useful when the fluid-flow domain is almost 2D, has perfect symmetry (e.g., axial symmetry), or the 3D geometry is too complex and hence too computationally demanding. For the last case, the difference between the "realistic" 3D geometry of the system under investigation and the "surrogate" 3D geometry represented by a 2D model should be fully appreciated in order to rationally predict fluid flow behavior.

This article aims at the development of a surrogate 2D CFD model for reliable prediction of gastric emptying, which is critical for understanding the digestion process. The motivation for such development is first justified by the significant overestimation of emptying rate by a conventional 2D model. Respecting the difference between the 3D realistic and surrogate geometries, to achieve equivalent emptying rate, we then develop a mapping approach that can convert measured dynamic data on pyloric diameter to pyloric size evolution in the 2D model. This surrogate model not only has high computational efficiency due to its 2D nature but also achieves emptying rate that is very close to the 3D model. At the same time, it can capture 3D flow behavior, such as retropulsive flow and recirculation eddies. Furthermore, the model demonstrates excellent generality for fluids with different properties, offering a powerful tool for gastric emptying studies.

1. Introduction

Gastric emptying is an essential step in the complete digestion process, involving gastric motility and the discharge of food in the stomach into the intestine. The food may be liquid, solid, or a mixture of two. After food intake, the proximal stomach relaxes to accommodate the food, while the distal stomach mixes the food and propels it toward the duodenum by peristaltic contraction (Phillips et al., 2015). Diseases such as dyspepsia and gastroparesis are associated with disorders in gastric emptying (Maurer, 2012). Therefore, quantitative assessment of gastric emptying rate is essential for the clinical diagnosis and treatment of gastric diseases.

To gain insights into this complex process, computational fluid dynamics (CFD) has emerged as a valuable tool for studying gastric emptying. Through CFD models, researchers were able to explore how factors like food properties (Harrison et al., 2018; Li et al., 2021), reduced gravity (Li et al., 2024), gastric surgery (Kuhar et al., 2024; Xu

et al., 2024), body posture (Lee et al., 2022) and gastric motility (Ebara et al., 2023; Kuhar et al., 2022) can quantitatively affect the emptying process. CFD simulations can offer spatially and temporally distributed high-resolution data on gastric flow patterns and emptying behavior that can lead to insights into the mechanics of digestion, which are difficult to be obtained from *in vivo* or *in vitro* experiments (Liu et al., 2024). However, because of the 3D irregular shape and complex motility of the stomach, developing a reliable model that can reproduce gastric emptying phenomena is very challenging.

Three-dimensional (3D) CFD models are more accurate than 2D models in capturing the stomach's realistic geometry. Nevertheless, despite their accuracy, simulations using 3D models are computationally demanding. For instance, Kamaltdinov et al. (2024) reported that simulating a 30-minute gastric emptying process in 3D could take over 300 h on a computer with 32 cores (AMD Opteron processors, 2.4 GHz). As a more computationally efficient approach, two-dimensional (2D) CFD models have traditionally been adopted for simulating gastric fluid

E-mail address: jie.xiao@suda.edu.cn (J. Xiao).

^{*} Corresponding author.

dynamics, despite certain limitations. Pal et al. (2004, 2007) developed a 2D model based on MRI images to analyze flow and mixing during gastric emptying. Their work revealed the "Magenstrasse" phenomenon, which captures a pathway that rapidly directs liquid gastric content from the fundus to the duodenum. Kozu et al. (2010) then used a simplified 2D model of the antral region to study how peristaltic contractions and fluid viscosity can influence gastric mixing. Trusov et al. (2013) developed a preliminary 2D model of the gastrointestinal tract to study the distribution of fragmented food particles in the stomach and the influence of antral contractions on gastric flow. Hao et al. (2015) simulated gastric emptying and the movement of gastroretentive microparticles under gravity using a 2D multiphase flow model. In one recent study, Toniolo et al. (2023) developed a 2D model based on fluid-structure interaction (FSI) analysis to study the effects of gastrectomy and food viscosity on gastroesophageal reflux, providing scientific guidance for surgical design optimization.

In 2D simulations involving gastric emptying, the emptying rate is typically controlled by the researchers in different ways, lacking scientific rigor. For example, in the model developed by Pal et al. (2004, 2007), gastric emptying rates were controlled by specifying changes in stomach volume over time to match physiological data — specifically, a 35 % volume reduction within 15 min after ingestion. Note that their model did not account for gravity, implying an emptying rate solely determined by the prescribed volume decrease. This approach allowed them to control the emptying rate by simply specifying how stomach volume changes over time. Without considering natural effect of gravity and motility on gastric emptying, this method has difficulty in characterizing the realistic fluid dynamics. Similarly, Hao et al. (2015) developed a 2D model to study gastric emptying and microparticle movement, specifying an outlet velocity to match physiologically measured emptying data. They set the pyloric outlet as a velocity outlet at 0.3 mm/s, which allowed the simulated gastric content to decrease by 35 % in $15 \min$. The same outlet velocity was used for all fluids with vastly different viscosities (1 cp and 16,384 cp). This approach cannot realistically capture the slow emptying process experienced by highviscosity fluids. Although these methods can match physiological data under specific conditions, the emptying rate depends on predefined settings, preventing realistic prediction of gastric emptying and limiting their general applicability.

Despite their high computational efficiency, conventional 2D models have a significant limitation in accurately capturing the opening dynamics of the pylorus—the outlet at the lower end of the stomach that serves as a valve, controlling outflow from the stomach to the small intestine. This limitation arises from the intrinsically geometrical differences between 2D and 3D models. The realistic gastric geometry is inherently three-dimensional and asymmetric. Its irregular "J"-shaped anatomy and complex structure make 2D simplifications particularly challenging and prone to error. The "realistic" 3D geometry of the stomach is depicted in Fig. 1(a), which captures the irregular "J"-shaped anatomy of the human stomach (Ferrua and Singh, 2010). However, a "surrogate" 3D geometry represented by a 2D model needs to be obtained by extruding the 2D cross-sectional geometry (on the *x-y* plane) in the *z* direction (see Fig. 1(b)).

Obviously, two geometries in Fig. 1 are significantly different. The pylorus in the "realistic" 3D geometry is circular in shape, while it becomes a rectangle in the "surrogate" 3D geometry. Note that, to maintain the same volume between the "surrogate" and "realistic" geometries, the extruded length of the rectangular pylorus must be significantly larger than its height (see Fig. 1(b)). Experimentally, the opening dynamics of the pylorus can be observed using magnetic resonance imaging (MRI) (Pal et al., 2004), which allows researchers and clinicians to measure the diameter of the pylorus as a function of time. Conventionally, this measured diameter has been used as the outlet size in stomach emptying simulations (Kuhar et al., 2022; Pal et al., 2007; Ferrua and Singh, 2010). This approach to set outlet size in a 2D stomach emptying model is essentially using the diameter of the circular pylorus

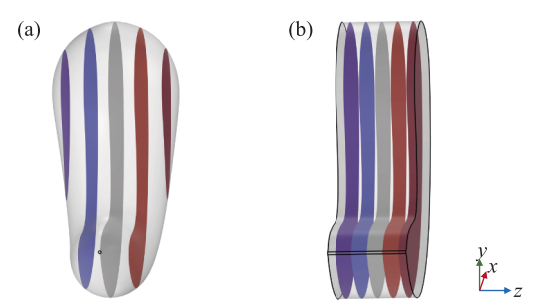


Fig. 1. 3D cross-sectional views of the stomach model: (a) the "realistic" 3D geometry of stomach represented by a 3D model, and (b) the "surrogate" 3D geometry represented by a 2D model. Note that the word "realistic" is used as a counterpart for "surrogate". The geometry in (a) is a simplified but representative geometry that has been widely adopted for modeling stomach. It indeed differs drastically from a realistic stomach, whose many detailed physiological features have been neglected.

as the height of the rectangular pylorus in the "surrogate" 3D geometry, which will drastically exaggerate the pyloric area. Consequently, such a setting in the 2D model would inevitably and significantly overestimate the gastric emptying rate. How to develop a 2D CFD model that can reliably predict gastric emptying has not been systematically and quantitatively addressed in previous studies, making it a key unresolved challenge. Even if the "surrogate" rectangular pylorus is adjusted to have the same area as the "realistic" circular pylorus, the geometric differences between the two shapes can result in distinct flow dynamics, further contributing to discrepancies in emptying rates between 2D and 3D models. Therefore, a critical challenge in developing a reliable 2D stomach emptying model lies in determining how to appropriately set the opening dynamics of the "surrogate" rectangular pylorus based on MRI-observed dynamic data on pyloric diameter. Addressing this challenge is essential for achieving accurate and rational predictions of gastric emptying rates by 2D models.

In this work, the above listed challenge has been rigorously addressed. The derivation of the opening dynamics of the "surrogate" rectangular pylorus based on MRI-observed pyloric diameter data is viewed as a mapping process, where the dynamic changes in the circular pyloric diameter are translated into the height of the "surrogate" rectangular pylorus (with a constant extruded length) to achieve equivalent emptying rates in 2D and 3D models. This methodology enables quantitatively consistent gastric emptying behavior with significantly reduced computational efforts. Detailed mapping approach will be delineated in the following text. The effectiveness and generality of the mapping approach will be demonstrated by case studies.

2. Size mapping from circular pylorus to "surrogate" rectangular pylorus

To facilitate methodology presentation and results analysis, five geometric models are defined for simulating gastric emptying: one 3D model and four 2D models. As shown in Fig. 2(a), with its pyloric region illustrated, the 3D model adopts the measured dynamic data of the pyloric diameter d_1 and serves as the ground truth. Fig. 2(b) presents the 2D models, where the top-left inset shows the pyloric sizes adopted in different 2D models. Note that, this size in the 2D model is essentially the height of the rectangular pylorus in the corresponding 3D equivalent geometry. The conventional 2D (C2D) model directly uses d_1 as the pyloric height. Direct use of d_1 can lead to the exaggeration of the pyloric area, as we have discussed above. In the surrogate 2D (S2D) model, the pyloric size is rigorously derived through a mapping method that translates d_1 into the height of the "surrogate" rectangular pylorus (d_2) . Additionally, two other 2D models are introduced for comparison. The H2D model uses a pyloric height d_3 derived by matching the hydraulic diameters of 2D and 3D models, while the A2D model obtains a pyloric

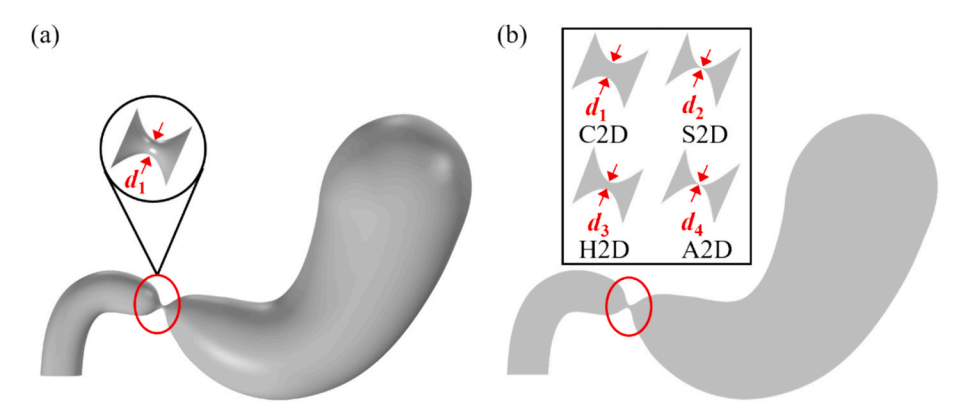


Fig. 2. Geometric structures of (a) the 3D model and its pyloric region, (b) 2D models with four different pyloric heights: the conventional 2D (C2D) model, the surrogate 2D (S2D) model, the 2D model with pyloric height (d_3) determined based on hydraulic diameter equivalence at the pyloric cross-section (abbreviated as H2D model), and the 2D model with pyloric height (d_4) determined based on pyloric cross-sectional area equivalence (abbreviated as A2D model).

height d_4 based on equal pyloric cross-sectional areas of two models.

In this study, an air-liquid two-phase flow model is employed to quantitatively capture the gastric emptying process. The level-set method is utilized to track the interface, ensuring reliable representation of the evolving gastric contents during emptying.

Mapping d_1 *to* d_2 . To derive the expression for mapped pyloric height (d_2), values of the following parameters and variables need to be specified or obtained: V_1 , V_1^{L0} , A, d_1 , p_{out} , ρ and μ . As shown in Fig. 3, V_1 is the initial volume of the 3D gastric model (m^3), V_1^{L0} is the initial liquid volume in the stomach, m^3 , A is the initial area of the S2D gastric model, i.e., the cross-sectional area of the "surrogate" 3D model (m^2), d_1 is the MRI-measured dynamic pyloric diameter (m), p_{out} is the outlet pressure (Pa), ρ is the fluid density (kg/ m^3) and μ is the fluid viscosity (Pa•s).

The "surrogate" 3D model extruded from the 2D model should maintain identical gastric volume with the 3D model:

$$V_1 = V_2 = A \cdot l \tag{1}$$

where V_2 is the initial volume of the "surrogate" 3D gastric model. Note that the gastric volume of the 3D stomach (V_1) can be obtained by integrating 1 over the total volume in stomach. Similarly, the area of the 2D stomach (A) can be obtained by integration as well.

The extruded length *l* becomes:

$$l = \frac{V_1}{A} \tag{2}$$

As shown in Fig. 3, the S2D model is extruded by length (*l*) to construct the geometry of the "surrogate" 3D model. To ensure an equal emptying rate between the S2D and 3D models, at a specific moment throughout the complete emptying process, both pyloric outlet flow rate and the volume of fluid left in the stomach should be identical for both

models. Mathematically, the following two equations should be satisfied simultaneously:

$$\begin{cases} Q_1^p = Q_2^p \\ V_1^L = V_2^L \end{cases}$$
 (3 and 4)

where Q_1^P and Q_2^P are pyloric outlet flow rate of the 3D and S2D models (m³/s), respectively, V_1^L and V_2^L represent the volume of fluid left in the stomach in the 3D model and the "surrogate" 3D model (m³), respectively. Specifically, V_1^L is obtained by integrating the 3D liquid domain in the stomach during 3D simulation of the emptying process, while V_2^L can be obtained by integration of the extruded length (I) over the 2D liquid domain in the stomach during S2D simulation of the emptying process. To ensure that Eq. (4) holds at the beginning of the emptying process, the initial gastric liquid area of the S2D model (m²), A_2^{L0} , must be determined first:

$$A_2^{10} = \frac{V_1^{10}}{l} \tag{5}$$

where V_1^{L0} represents the initial liquid volume in the three-dimensional model (m³).

Further expansion of Eq. (3) yields:

$$\overline{u_1} \cdot A_1^p = \overline{u_2} \cdot A_2^p \tag{6}$$

where $\overline{u_1}$ and $\overline{u_2}$ are the average pyloric outlet velocities of the 3D and S2D models (m/s), A_1^P and A_2^P are the areas of the circular pylorus in the 3D model and the "surrogate" rectangular pylorus in the S2D model (m²), respectively. In the 3D simulation of gastric emptying process, $\overline{u_1}$ is determined by integrating the velocity over the pyloric cross-section and dividing by A_1^P , whereas in the S2D simulation, $\overline{u_2}$ is calculated by

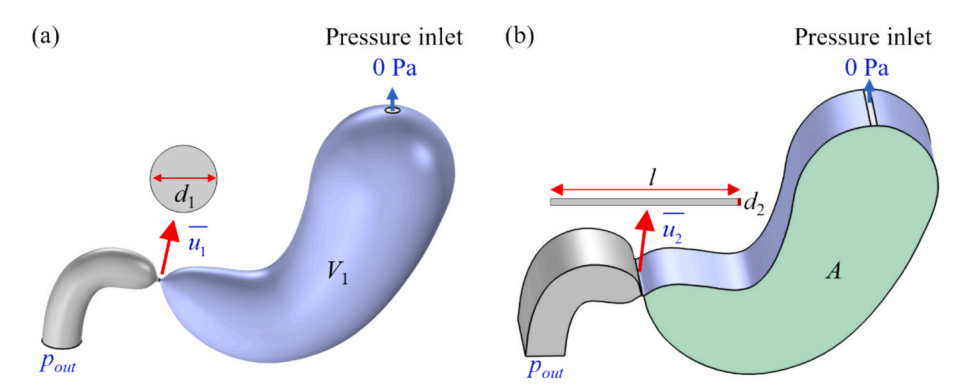


Fig. 3. Geometries of: (a) the 3D model, and (b) the "surrogate" 3D model extruded from the S2D model. In the 3D model, the diameter of the circular pylorus is d_1 . In the surrogate 3D model, the pylorus becomes a rectangle with height d_2 and extruded length l.

integrating the velocity over the pyloric region and dividing by the pyloric height (d_2). Specifically, $A_1^P = \pi d_1^2/4$ for the 3D model and $A_2^P = l \cdot d_2$ for the S2D model. This yields the following equation:

$$\overline{u_1} \cdot \frac{\pi d_1^2}{4} = \overline{u_2} \cdot l \cdot d_2 \tag{7}$$

As a narrow passage connecting the stomach to the duodenum, the pylorus has a cross-sectional area much smaller than that of the antrum. The sudden reduction in flow area induces substantial energy dissipation. For such small-orifice flow, a discharge coefficient is typically introduced to account for flow energy losses (Alajmi et al., 2019). This coefficient can be used to compensate discrepancies in flow dynamics arising from the geometric differences between the circular pylorus in the 3D model and the rectangular pylorus in the S2D model. This geometric difference leads to differences in the velocities at the orifice, $\overline{u_1} \neq \overline{u_2}$, even when the cross-sectional areas A_1^P and A_2^P are the same. In the 3D model, the discharge coefficient is used to express the average pyloric outlet velocity $(\overline{u_1})$ as:

$$\overline{u_1} = C_{d1} \cdot \overline{u_1^0} \tag{8}$$

where C_{d1} represents the discharge coefficients in the 3D model. $\overline{u_1^0}$ presents the theoretical average pyloric outlet velocity without energy losses in the 3D model (m/s). Notably, in the S2D model, the average pyloric outlet velocity ($\overline{u_2}$), can be directly obtained from the 2D simulation during the gastric emptying process, eliminating the need to use the discharge coefficient for its calculation. Substituting Eq. (8) into Eq. (7), the expression for d_2 can be obtained:

$$d_2 = \frac{\pi d_1^2}{4l} \cdot \frac{C_{d1} \overline{u_1^0}}{\overline{u_2}} \tag{9}$$

According to this equation, determining d_2 requires the discharge coefficient (C_{d1}) and the theoretical pyloric outlet velocity $(\overline{u_1^0})$ from the 3D model, where $\overline{u_1^0}$ can be determined using Bernoulli's equation:

$$gz_a + \frac{(\overline{u_a})^2}{2} + \frac{p_a}{\rho} = gz_0 + \frac{(\overline{u_1^0})^2}{2} + \frac{p_0}{\rho}$$
 (10)

where z_a and z_0 are the liquid levels (m) at the liquid surface and pylorus, respectively, with the height difference between them denoted as $h_a=z_a-z_0,\,p_a$ and p_0 are the corresponding pressures (Pa), $\overline{u_a}$ is the average velocity at the liquid surface (m/s) (see Fig. 4). Given that the cross-sectional area of the pyloric orifice is much smaller than that of the gastric body, the velocity at the liquid surface can be safely neglected, i. e., $\overline{u_a}=0$ m/s. Additionally, $p_a=0$ Pa. Therefore, the expression for the theoretical average pyloric outlet velocity can be simplified to:

$$\overline{u_1^0} = \sqrt{2\left(gh_a - \frac{p_0}{\rho}\right)} \tag{11}$$

where h_a is the height difference between the pylorus and the liquid

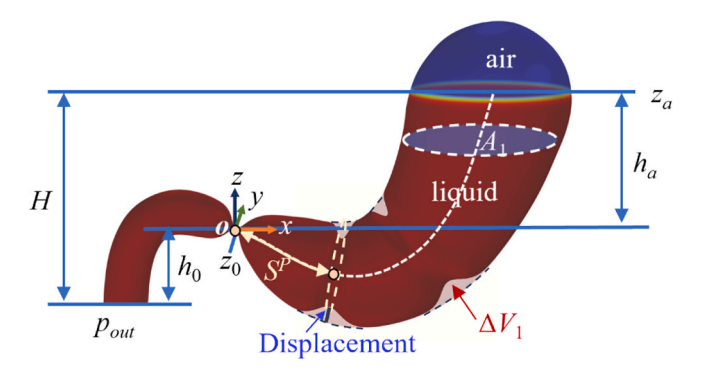


Fig. 4. Illustration of $\overline{u_1^0}$ calculation based on Bernoulli's equation.

surface (m). With p_0 simplified to $p_0 = p_{out} - \rho g h_0$, where h_0 is the height difference between the pylorus and the outlet (m), leading to the subsequent expression for $\overline{u_0^0}$:

$$\overline{u_1^0} = \sqrt{2\left(gH - \frac{p_{out}}{\rho}\right)} \tag{12}$$

where H is the height difference between the liquid surface and the outlet (m) (see Fig. 4), which varies over time during the gastric emptying process due to both the decrease of liquid volume left in the stomach and the change of gastric volume induced by antral contraction waves (ACWs). Therefore, H can be written as:

$$H = H_1 + \Delta H_1 \tag{13}$$

where H_1 is the liquid height in the absence of ACWs (m), determined solely by the gastric liquid volume (V_1^L) . ΔH_1 is the additional height caused by ACWs (m). For a specific 3D geometry of the stomach, the liquid height without ACWs can be readily derived from the gastric liquid volume in the 3D model (m³) as:

$$H_1 = f_1(V_1^L) (14)$$

The specific form of Eq. (14) can be straight-forwardly determined through data fitting.

As shown in Fig. 4, the periodic contraction of ACWs leads to instantaneous changes in gastric cavity volume (ΔV_1), resulting in liquid surface fluctuations (ΔH_1). To quantify this dynamic effect, the relationship between volume change and height variation needs to be established:

$$\Delta H_1 = \frac{\Delta V_1}{A_1} \tag{15}$$

where A_1 is the average horizontal cross-sectional area of the gastric cavity (m²) (see Fig. 4). ΔV_1 is calculated as the difference between the gastric cavity volume at a given time and the initial gastric cavity volume (V_1) during the gastric emptying process. A_1 can be approximated as the derivative of gastric liquid volume (V_1) with respect to the liquid height without ACWs (H_1):

$$A_1 = \frac{dV_1^L}{dH_1} = \frac{1}{f_1(V_1^L)} \tag{16}$$

Since ACWs propagate with a fixed cycle (20 s) (Pal et al., 2004), ΔV_1 varies cyclically with time and can be expressed as a time-dependent cyclic function:

$$\Delta V_1 = f_2(t) \tag{17}$$

The relationship between ΔV_1 and time (t) can be determined through 3D emptying simulations. Consequently, ΔH_1 can be expressed as:

$$\Delta H_1 = f_1'(V_1^L) \cdot f_2(t) \tag{18}$$

By substituting Eq. (14) and Eq. (18) into Eq. (13), H can be determined. The calculated H can then be substituted into Eq. (12), yielding the theoretical average pyloric outlet velocity $(\overline{u_0^0})$:

$$\overline{u_1^0} = \sqrt{2\left(g\left(f_1\left(V_1^L\right) + f_1\left(V_1^L\right) \cdot f_2(t)\right) - \frac{p_{out}}{\rho}\right)}$$
(19)

The V_1^L can be substituted by the V_2^L according to Eq. (4), yielding:

$$\overline{u_1^0} = \sqrt{2\left(g(f_1(V_2^L) + f_1(V_2^L) \cdot f_2(t)) - \frac{p_{out}}{\rho}\right)}$$
 (20)

Based on the recorded time instants (t) and the corresponding gastric liquid volume (V_2^L) during the S2D emptying simulation, along with values of p_{out} and ρ , the theoretical average pyloric outlet velocity $(\overline{u_1^0})$ can be calculated.

So far, the only unknown in Eq. (9) is C_{d1} , i.e., the discharge coefficient in the 3D model. At low Reynolds numbers, the discharge coefficient is proportional to the square root of the Reynolds number, while it tends to become constant at high Reynolds numbers. This relationship can be expressed by the empirical formula proposed by Wu et al. (2002):

$$C_{d1} = f(Re_1) = C_{d\infty} \left(1 + ae^{-\frac{\delta_1}{C_{d\infty}}\sqrt{Re_1}} + be^{-\frac{\delta_2}{C_{d\infty}}\sqrt{Re_1}} \right)$$
(21)

where Re_1 is the Reynolds number of the 3D model, $C_{d\infty}$ represents the discharge coefficient for a specific orifice under turbulent flow, and a,b, δ_1 , δ_2 are orifice-specific coefficients. These parameters can be determined by fitting the relationship between C_{d1} and $\sqrt{Re_1}$, subject to the constraint $C_{d1}|_{\sqrt{Re_1}=0}=1+a+b=0$ (Wu et al., 2002). The Reynolds number (Re_1) is expressed as:

$$Re_1 = \frac{d_1 \overline{u_1} \rho}{\mu} \tag{22}$$

It should be noted that the diameter used to calculate the Reynolds number should be the hydraulic diameter. Given that the pyloric orifice in the 3D model exhibits a circular cross-section, the hydraulic diameter equals the pyloric diameter (d_1) .

To obtain discharge coefficient (C_{d1}) data for a complete feasible range of Reynolds numbers (Re_1) in the 3D model, simulations of gastric emptying for the 3D model are required. As the Reynolds number dynamically evolves due to the periodic variation of both the pyloric diameter (d_1) and the average pyloric outlet velocity $(\overline{u_1})$ during gastric emptying, a single simulation can only cover a certain range of the Reynolds number. A strategy is developed to design 3D simulation cases, so that the complete feasible range of Reynolds numbers can be covered with minimized number of 3D simulations. First, perform a simulation using a low-viscosity fluid (starting at 0.001 Pa·s, which falls at the lower end of the viscosity range for common liquid foods) to cover the upper Reynolds number range at high emptying velocities; if the lowviscosity simulation does not adequately cover the low Reynolds number range, then conduct an additional simulation with a higher-viscosity fluid. Note that, even for one specific viscosity, in one emptying simulation case, Reynolds number evolves with time due to the dynamic change of both d_1 and $\overline{u_1}$ By adjusting fluid viscosity, the range of Reynolds number that can be covered by one simulation can be systematically shifted—low-viscosity simulations capture the mid-to-high Reynolds number range, whereas high-viscosity simulations tend to sample the low Reynolds number region. Assuming that gastric emptying flow remains laminar and the discharge coefficient exhibits a piecewise continuous relationship with the Reynolds number in the laminar regime (stabilizing at high Reynolds numbers while following a linear trend at low Reynolds numbers (Wu et al., 2002)), two representative cases of gastric emptying simulations for the 3D model with different viscosities can be sufficient to cover the required Re1 range for deriving a general equation of C_{d1} by data fitting.

During 3D simulations of gastric emptying, the pyloric diameter (d_1) and the average pyloric outlet velocity $(\overline{u_1})$ at different time instants (t) were recorded, along with the specified values of material property parameters: ρ and μ , allowing the calculation of the corresponding Reynolds number (Re_1) using Eq. (22). Additionally, the gastric liquid volume (V_1^L) at each selected time instant (t) was recorded, and using Eq. (19), the theoretical average pyloric outlet velocity of the 3D model $(\overline{u_1^0})$ was calculated. This value was then substituted into Eq. (8) to determine the corresponding discharge coefficient (C_{d1}) . The obtained discharge coefficients were then fitted to the formula given by Eq. (21), subject to the constraint condition, to determine the characteristic parameters $C_{d\infty}$, a, b, δ_1 and δ_2 .

Since Eq. (22) includes the 3D pyloric outlet average velocity $(\overline{u_1})$, it must be reformulated in order to be used in gastric emptying simulations

of the S2D model. According to Eq. (8), $\overline{u_1}$ can be expressed in terms of the discharge coefficient (C_{d1}) and the theoretical average velocity ($\overline{u_1^0}$), yielding:

$$Re_1 = \frac{d_1 C_{d1} \overline{u_1^0} \rho}{u} \tag{23}$$

Substituting Eq. (23) into Eq. (21) yields the implicit expression for C_{d1} :

$$C_{d1} = C_{d\infty} \left(1 + ae^{-rac{\delta_1}{C_{d\infty}}} \sqrt{rac{d_1 C_{d1} \overline{u}_1^0
ho}{\mu}} + be^{-rac{\delta_2}{C_{d\infty}}} \sqrt{rac{d_1 C_{d1} \overline{u}_1^0
ho}{\mu}}
ight)$$
 (24)

In the gastric emptying simulation of the S2D model, the gastric liquid volume (V_2^L) and the average pyloric outlet velocity $(\overline{u_2})$ can be obtained from the simulation results and processed at each time instant (t). With V_2^L , t, and p_{out} , $\overline{u_1^0}$ can be calculated using Eq. (20). Then, with known d_1 , $\overline{u_1^0}$, ρ , and μ , the discharge coefficient (C_{d1}) can be determined from Eq. (24). Finally, by substituting d_1 , l, C_{d1} , and $\overline{u_2}$ into Eq. (9), the corresponding pyloric height (d_2) is finally obtained. It should be noted that the value of d_2 calculated at each time instant is used as the input for the next time instant, enabling dynamic updating of the pyloric height in the S2D model throughout the entire simulation.

Derivation steps for d_2 . In summary, the mapped pyloric height (d_2) can be systematically determined through the following steps:

Step 1: Geometric construction

Construct 3D and 2D gastric geometries. The 2D geometry is the central vertical cross-section of the 3D gastric geometry (see Fig. 2).

Step 2: System specification

Specify or obtain the values for the following variables and parameters. Obtain the gastric volume of the 3D stomach (V_1) and area of the 2D stomach (A_1) through integration. Furthermore, specify initial gastric liquid volume (V_1^{L0}) , dynamic pyloric diameter (d_1) , which can be the MRI data), outlet pressure (P_{out}) , liquid density (ρ) and viscosity (μ) .

Step 3: Calculate the extruded length (1)

Calculate the extruded length (l) of the S2D model using Eq. (2) (see Fig. 3(b)).

Step 4: Initialize two-phase domains

Determine the initial liquid area (A_1^{L0}) in the S2D model based on the extruded length (I), using Eq. (5).

Step 5: Derive the relationship between V_1^L and H_1

For a specific 3D gastric geometry, without consideration of ACWs, one gastric liquid volume (V_1^L) corresponds to one liquid height (H_1) . Their quantitative relationship (Eq. (14)) can be obtained through data fitting. Then, derive the expression for the average horizontal cross-sectional area of the gastric body (A_1) using Eq. (16).

Step 6: Perform 3D gastric emptying simulations (2 representative cases)

Perform up to two 3D gastric emptying simulations by varying the fluid viscosity (e.g., two cases with low and high viscosities respectively) while keeping the density constant. Record and obtain the average pyloric outlet velocity $(\overline{u_1})$, pyloric diameter (d_1) , gastric liquid volume (V_1^L) , and the change of gastric cavity volume (ΔV_1) at all time instants (t).

Step 7: Determine the expression of theoretical average pyloric outlet velocity $(\overline{u_1^0})$

During the 3D simulation in Step 6, the recorded ΔV_I and time (t) data are used to establish a cyclic interpolation function as defined in Eq. (17). This function is then utilized to derive ΔH_1 in Eq. (18), and further the theoretical average pyloric outlet velocity ($\overline{u_1^0}$) (Eq. (19)). Equation (19) can be expressed in the form of Eq. (20). Note that Eq. (19) is used for subsequent derivation of the discharge coefficient C_{d1} ; while Eq. (20), obtained by replacing V_1^L with V_2^L , will be used for calculating $\overline{u_1^0}$

in the S2D gastric emptying simulation.

Step 8: Obtain the expression of the discharge coefficient (C_{d1})

Using the values of $\overline{u_1}$, t, V_1^L from Step 6, along with the input parameters $(\rho, \mu, p_{out}, d_1)$, calculate a series of theoretical average pyloric outlet velocity $(\overline{u_1^0})$ and Reynolds numbers (Re_1) based on Eq's. (19) and (22), respectively. Then substitute $\overline{u_1}$ and $\overline{u_1^0}$ into Eq. (8) to obtain the corresponding discharge coefficient (C_{d1}) . Based on the calculated $\sqrt{Re_1} - C_{d1}$ data pairs at all time instants, Eq. (21) is fitted under the constraint (1 + a + b = 0) to determine the characteristic parameters $(C_{d\infty}, a, b, \delta_1, \delta_2)$. Finally, the discharge coefficient C_{d1} is expressed in the form of Eq. (24).

Step 9: Establish the equation for calculating the mapped pyloric height (d_2)

With $\overline{u_1^0}$ and C_{d1} derived in Steps 7 and 8 (i.e., Eq's. (20) and (24)), Eq. (9) becomes an explicit equation for the mapped pyloric height d_2 . **Step 10:** Perform gastric emptying simulation using the S2D model

By using the values of $\overline{u_2}$ and V_2^L at each time instant (t), along with the prescribed variables and parameters $(\rho, \mu, p_{out}, d_1)$ and the extruded length (l), Eq. (9) can be utilized to dynamically update the mapped pyloric height (d_2) throughout the 2D simulation.

Note that, in the above procedure, steps 1–9 are performed only once to derive the general expressions for $\overline{u_1^0}$ (Eq. (20)) and C_{d1} (Eq. (24)). These expressions are established based on a fixed gastric geometric configuration and remain valid even when material properties are subsequently modified. Therefore, after changing gastric contents (with different ρ and μ), only Step 10 needs to be executed, by substituting the updated parameters into the established expressions.

Derivation of d_3 and d_4 . For comparison purposes, the pyloric heights for the H2D and A2D models are derived based on different equivalence assumptions. For the H2D model, the pyloric height (d_3) is determined by equating the hydraulic diameter of the 3D model's circular pylorus to that of the H2D model's rectangular pylorus, which can be expressed as:

$$d_1^h = d_3^h \tag{25}$$

where d_1^h is the hydraulic diameter of the circular pylorus in the 3D model (i.e., d_1), m. d_3^h is the hydraulic diameter of the rectangular pylorus, m, which is given by:

$$d_3^h = \frac{4l \cdot d_3}{2(l+d_3)} \tag{26}$$

where $l \cdot d_3$ represents the area of the rectangular pylorus (m²), 2 ($l + d_3$) represents the wetted perimeter of the rectangular pylorus (m). Substituting Eq. (26) into Eq. (25) yields:

$$d_1 = \frac{2l \cdot d_3}{l + d_3} \tag{27}$$

Thus, the pyloric height for the H2D model (d_3) is simply:

$$d_3 = \frac{l \cdot d_1}{2l - d_1} \tag{28}$$

The pyloric height of the A2D model (d_4) is determined based on the assumption of equivalent pyloric cross-sectional areas between the 3D model and the A2D model, which can be expressed as:

$$A_1^P = A_4^P \tag{29}$$

where A_4^P is the pyloric cross-sectional area of the A2D model, m². Then the following equation can be written:

$$\frac{\pi d_1^2}{4} = l \cdot d_4 \tag{30}$$

Thus, the pyloric height for the A2D model (d_4) can be determined as:

$$d_4 = \frac{\pi d_1^2}{4l} \tag{31}$$

3. Results and Discussion

To demonstrate the reliability and generality of the S2D model, we will rigorously compare its performance with other models (3D, C2D, H2D, and A2D) in terms of gastric emptying behavior. Fluid properties (ρ, μ) will be varied, and the dynamic mapping method will be used to calculate corresponding pyloric heights (d_2) . The predicted emptying results from the S2D model will then be compared with those from the validated 3D model, which serve as the ground truth. Additionally, the computational time for both the S2D and 3D models will be compared to assess the advantages of the S2D model in terms of both prediction accuracy and computational efficiency.

To validate the S2D model, gastric emptying of water was selected as the base case for simulation. As shown in Fig. 5, a S2D geometry was first constructed as the central vertical cross-section of the 3D geometry. Following step 2, the gastric volume of the 3D stomach (V_1) is obtained (i.e., 8.9528×10^{-4} m³), which aligns with the physiological range of postprandial gastric volume (0.7-1.6 L) (Csendes and Burgos, 2005). The cross-sectional area (A) of the S2D model is 1.6123×10^{-2} m². Then specify initial gastric liquid volume (V_1^{L0}) , dynamic pyloric diameter (d_1) , outlet pressure (p_{out}) , liquid density (ρ) and viscosity (μ) . For the 3D model, the initial gastric liquid volume (V_1^{L0}) is set to 7.22×10^{-4} m³, accounting for 80 % of the total gastric cavity volume. The measured pyloric diameter(d_1), is modeled to open every 20 s for 2 s, with a diameter of 0.002 m during the opening phase (Ishida et al., 2019; Kuhar et al., 2022; Eyre-Brook et al., 1983). The pyloric diameter is set to 5 \times 10⁻⁴ m to indicate the closure state of the pylorus. Periodic opening and closure of the pylorus is activated at 48 s, corresponding to the time when the first ACW reaches the distal antrum (Ishida et al., 2019). The gastric inlet is open to air (i.e., 0 Pa), and the outlet pressure p_{out} is set to 400 Pa (Harrison et al., 2018), both of which are gauge pressures. The liquid has a density (ρ) of 1000 kg/m³ and a viscosity (μ) of 0.001 Pa·s.

According to Step 3, the extruded length of the rectangular pylorus (*I*) was calculated as 55.53×10^{-3} m. With the extruded length (*I*), the S2D model essentially represents a "surrogate" 3D geometry (see Fig. 3 (b)).

In the 4th step, the initial gastric liquid area (A_2^{L0}) of the S2D model was determined according to Eq. (5). A_2^{L0} is 1.3×10^{-2} m² in this study. The initial phase distributions for both 3D and S2D models are shown in Fig. 5.

Following Step 5, the relationship between liquid height without ACWs (H_1) and gastric liquid volume (V_1^L) in the 3D geometry can be fitted using a quadratic polynomial (see Fig. 6, $R^2 = 1.0000$):

$$H_1 = f_1(V_1^L) = -63681.9430(V_1^L)^2 + 238.1158V_1^L - 0.0248$$
 (32)

Given the high correlation ($R^2 = 0.9987$) between H_1 and V_1^L in the linear fit (Fig. 6), the inverse of the slope k (k = 170.4618) was adopted to approximate the average horizontal cross-sectional area of the gastric body (A_1) as a constant, thereby simplifying calculations.

According to Step 6, the gastric emptying simulation of a fluid with a low viscosity (i.e., 0.001 Pa·s) was first performed using the 3D model. The average pyloric outlet velocity ($\overline{u_1}$), gastric liquid volume (V_1^L), and the change of gastric cavity volume (ΔV_1) at different time instants (t) were recorded.

In the 7th step, using the recorded ΔV_1 and time (t) data, along with A_1 obtained in Step 5. The expression of the additional height caused by ACWs (ΔH_1) (Eq. (18)) can be determined as:

$$\Delta H_1 = 170.4618 f_2(t) \tag{33}$$

As shown in Fig. 7, ΔH_1 (represented as $k\Delta V_1$) exhibited periodic oscillations synchronized with antral contraction waves (ACWs). In addition, to validate this approximation method, the actual liquid height (H) and gastric liquid volume (V_1^L) were obtained from 3D gastric emptying simulation. Substituting V_1^L into Eq. (32) yielded H_1 , and the actual ΔH_1 (H- H_1) was compared with the approximation ($k\Delta V_1$) in

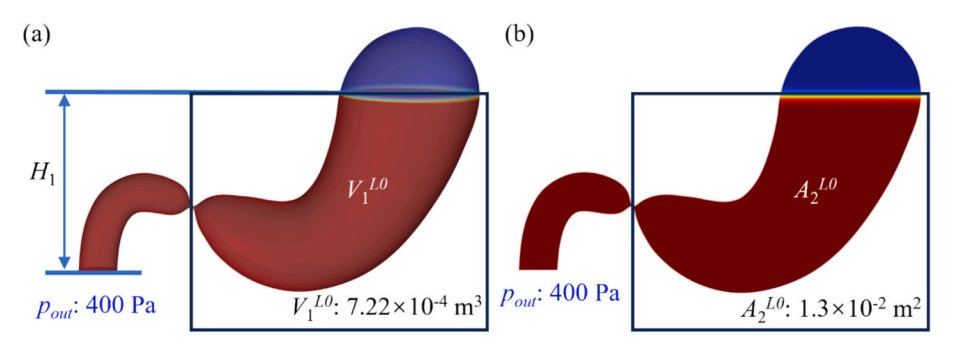


Fig. 5. Geometries and initial phase distributions in two models: (a) the 3D model; (b) the surrogate 2D (S2D) model (red regions indicate the liquid phase and blue regions denote the gas phase). (For interpretation of the references to colour in this figure legend, the reader is referred to the web version of this article.)

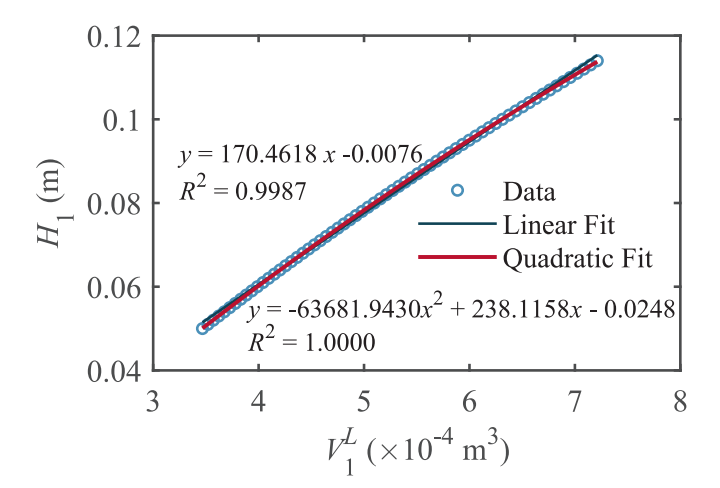


Fig. 6. Relationship between gastric liquid volume in the 3D stomach (V_1^L) and the liquid height without ACWs (H_1) , including both linear and quadratic fits. The inverse of the slope k from the linear fit approximates the average horizontal cross-sectional area of the gastric body (A_1) that can be used for subsequent calculation of ΔH_1 . The quadratic fit, which shows an excellent match with the data $(R^2 = 1.0000)$, is used for the calculation of H_1 . The gastric liquid volume (V_1^L) ranges from 3.61×10^{-4} m³ to 7.22×10^{-4} m³, representing the half-emptying and the initial gastric liquid volume, respectively.

Fig. 7(a). The consistency between H- H_1 and $k\Delta V_1$ confirmed the validity of the method.

Thus, the expression for the theoretical average pyloric outlet velocity $(\overline{u_1^0})$ can be determined as:

$$\overline{u_1^0} = \sqrt{2\left(g(f_1(V_1^L) + 170.4618f_2(t)) - \frac{p_{out}}{\rho}\right)}$$
 (34)

In the gastric emptying simulations using the S2D model, V_1^L in Eq. (34) can be substituted by V_2^L based on Eq. (4):

$$\overline{u_1^0} = \sqrt{2\left(g(f_1(V_2^L) + 170.4618f_2(t)) - \frac{p_{out}}{\rho}\right)}$$
 (35)

In the next step, using the recorded values from Step 6 ($\overline{u_1}$, V_1^L , t), along with the specified parameters (ρ , μ , p_{out} , d_1) to calculate the corresponding Reynolds number (Re_1) and discharge coefficient (C_{d1}).

As shown in Fig. 8, gastric emptying of the low-viscosity fluid (0.001 $Pa \cdot s$) covered the high Reynolds numbers region (see the filled circles). Note that, each filled circle represents the data at one specific time instant during the emptying simulation. Colors filled in the circle represent those sampling time instants.

Subsequently, the viscosity was increased to 0.01 Pa·s, repeating Steps 6 and 8 to extend the coverage to the low-Reynolds-number region. Since the general formula for $\overline{u_1^0}$ has already been established, only these two steps need to be repeated. The $\sqrt{Re_1} - C_{d1}$ relationship exhibits an initial linear growth followed by a plateau. Similar gastric emptying behavior was observed *in vivo* for fluids with different viscosities (Marciani et al., 2000), where the range of Re_1 during emptying resides within the plateau region of C_{d1} .

The fitted expression for C_{d1} is:

$$C_{d1} = 0.8129 \left(1 + 8.1012 e^{-0.0814 \sqrt{Re_1}} - 9.1012 e^{-0.0901 \sqrt{Re_1}} \right)$$
 (36)

It can be further expressed as an implicit equation for C_{d1} :

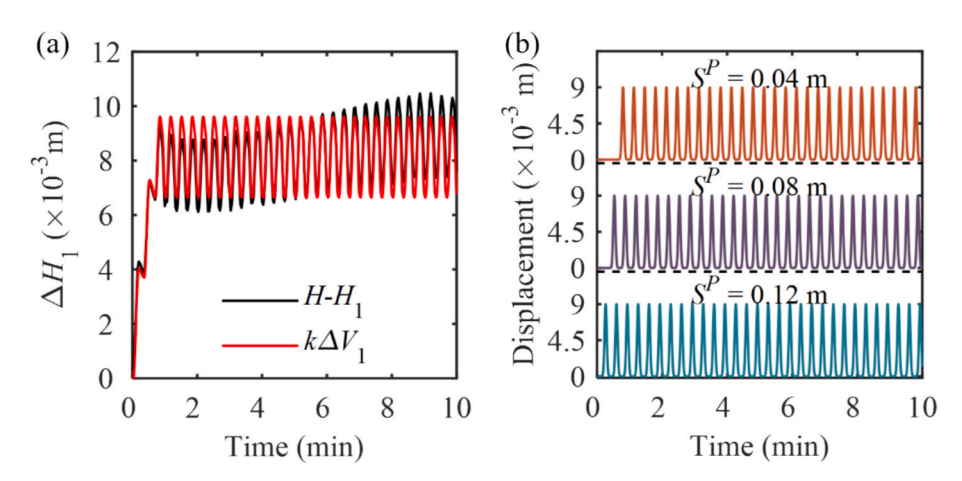


Fig. 7. Temporal evolutions of (a) the increased liquid height caused by ACWs (ΔH_1) and (b) the stomach wall displacement caused by the ACWs at different positions, where S^P represents the arc length measured along the stomach's centerline (m) (see Fig. 4). The periodicity of ΔH_1 corresponds to that of the ACWs, which has a period of 20 s (Pal et al., 2004).

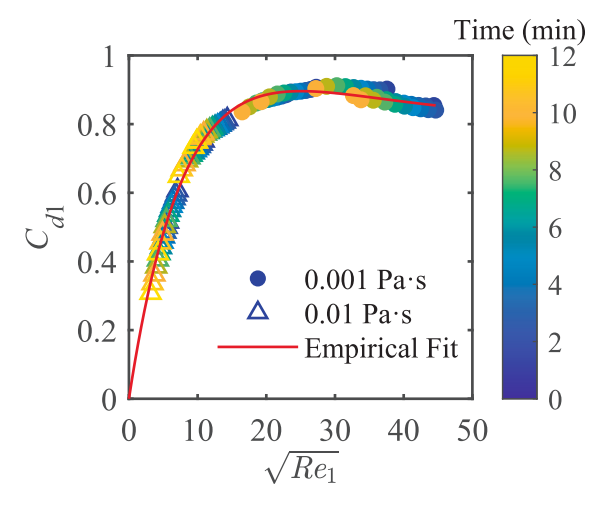


Fig. 8. The fitted curve for the discharge coefficient in the 3D model (C_{d1}).

$$C_{d1} = 0.8129 \left(1 + 8.1012e^{-0.0814\sqrt{\frac{d_1C_{d1}\overline{u_1^n}\rho}{\mu}}} - 9.1012e^{-0.0901\sqrt{\frac{d_1C_{d1}\overline{u_1^n}\rho}{\mu}}} \right)$$
(37)

In Step 9, the pyloric height (d_2) in the S2D model can ultimately be obtained by simultaneously solving Eq's. (9), (35), and (37). Subsequently, the S2D gastric emptying simulations can be performed. In the water emptying simulation, the resulting pyloric height (d_2) as a function of time is plotted in Fig. 9(b). As one can see, d_2 is significantly smaller than d_1 (Fig. 9(a)), with a maximum difference reaching up to 28-fold. As the emptying progresses, d_2 gradually increases during the early phase and this trend becomes more prominent towards the end. Specifically, the maximum pyloric opening increases from 7.1×10^{-5} m in the beginning to 15.8×10^{-5} m at the end, approximately doubled in magnitude. This dynamic adjustment of the pyloric height is the key to achieve consistent emptying rate as that of the 3D model.

A comparison of liquid heights between the 3D and S2D models (see

Fig. 10) reveals that, although the overall emptying time are nearly identical (maximum time difference of 0.4 min), there are notable differences in liquid heights at the same intragastric volume during emptying. Initially, with the same liquid volume, the liquid height difference is about 1 mm, but this number gradually increases and reaches 18 mm when 50 % of the liquid has been emptied. This discrepancy primarily arises from differences in geometric structure: the 3D model features a realistic J-shaped anatomy, with a narrower cavity near the pylorus and most of the liquid resides in the mid-stomach, while the S2D model maintains a constant cross-sectional area along the extruded direction, resulting in a more uniform volume distribution. The lower liquid height in the S2D model reduces the pressure difference that drives the flow, leading to a lower pyloric outflow velocity. To compensate and maintain an equivalent emptying rate with the 3D model, the S2D model dynamically increases the pyloric height (d_2) based on our mapping method, thereby enlarging the outlet flow area (A_2^P) . This trend in liquid height difference helps explain the observed increase of d_2 with time shown in Fig. 9(b).

The validity and effectiveness of the mapping method can be demonstrated by comparing the S2D simulation results with experimental data and those predicted by other representative 2D (i.e., C2D, H2D, and A2D) and 3D models. As shown in Fig. 11, the conventional 2D (C2D) model, which directly uses the measured diameter (d_1) as the pyloric height (Fig. 11(a) and (b)), greatly overestimates the pyloric size, resulting in a drastically short half-emptying time ($t_{1/2} = 20$ s) (Fig. 11 (c)), nearly 30 times faster than that of the 3D model ($t_{1/2} = 9.8 \text{ min}$). In contrast, the S2D model, which adopts the mapped height (d_2) , achieves a $t_{1/2}$ of 10.2 min, closely matching the prediction by the 3D model. For the H2D model, the value of d_3 is approximately one half of d_1 and significantly larger than d_2 , resulting in an excessively fast emptying rate $(t_{1/2} = 41 \text{ s})$, indicating that simply matching hydraulic diameters cannot ensure equivalent emptying behavior. Notably, the $t_{1/2}$ of both the C2D and H2D models are within 0.8 min, corresponding to the pyloric closure stage. At this stage, the 3D model exhibits negligible liquid discharge ($d_1 = 5 \times 10^{-4}$ m), whereas the C2D and H2D models predict rapid emptying even under comparable or smaller pyloric heights. For the A2D model, its pyloric height (d_4) differs from d_2 by less than 2 \times 10⁻⁵ m (Fig. 11(a) and (b)), yet the predicted emptying rate is substantially lower (see red and blue lines in Fig. 11(c)). Compared to the

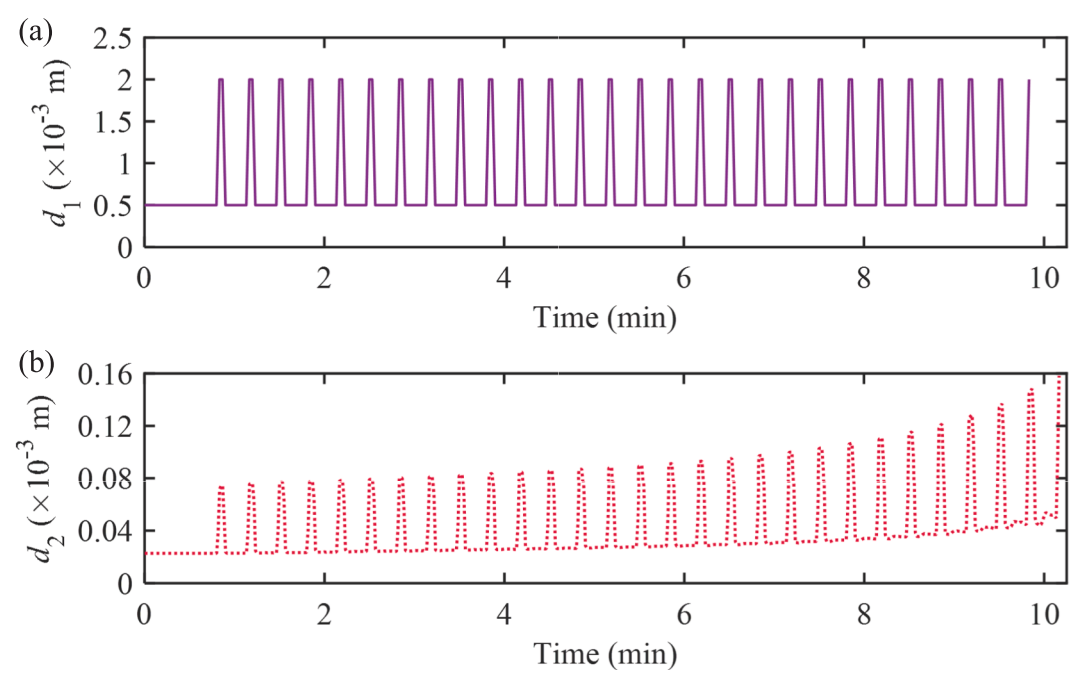


Fig. 9. Evolution of the pyloric size in the (a) 3D model (d_1) and (b) S2D model (d_2) during gastric emptying of water.

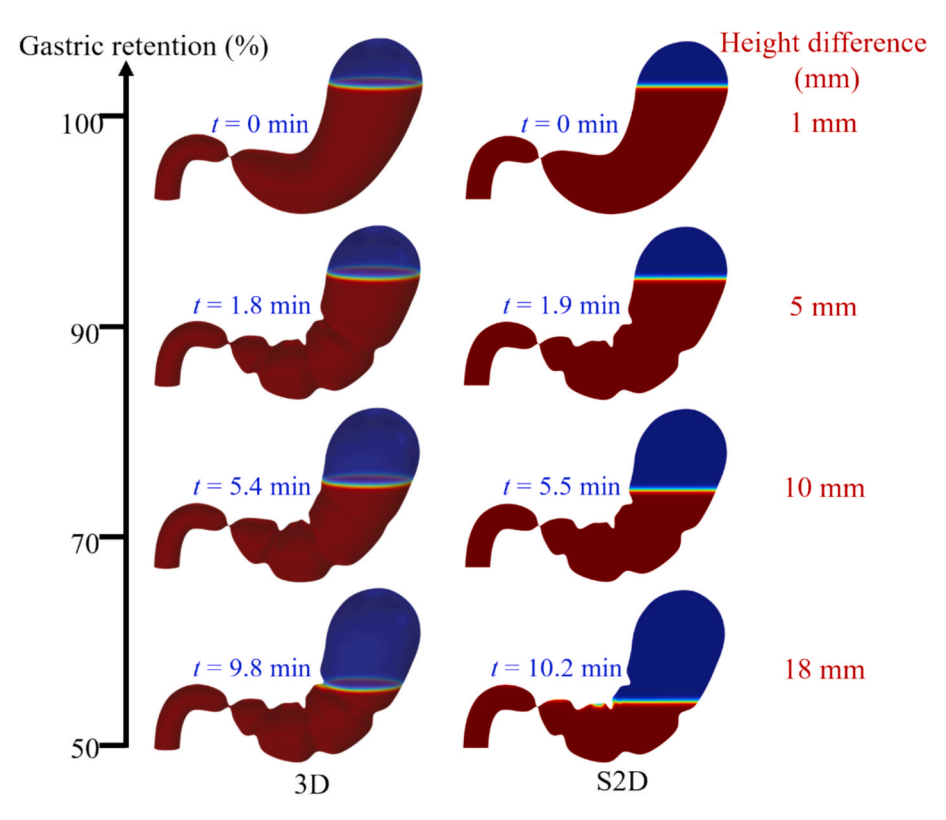


Fig. 10. Comparison of liquid heights at the same gastric retention between 3D and S2D models during gastric emptying of water.

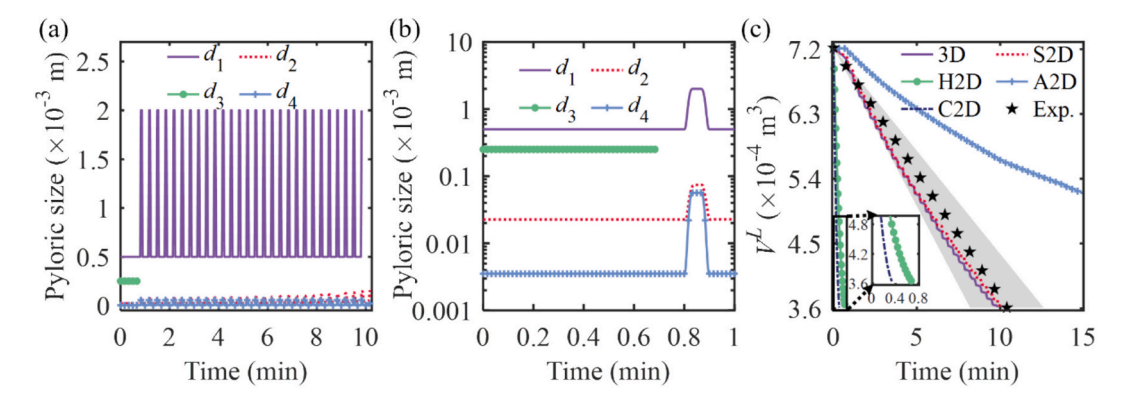


Fig. 11. Gastric emptying simulation results by different models and comparison with experimental data: (a) pyloric size evolution over time for the 3D (d_1) , C2D (d_1) , S2D (d_2) , H2D (d_3) and A2D (d_4) models; (b) pyloric size evolution during the initial 1 min, where the *y*-axis uses a logarithmic scale for pyloric size; (c) comparison between the predicted gastric emptying curves and *in vivo* experimental data (George, 1968), where the stars and the shaded area represent the average and the standard deviation of experimental data respectively. Note that the gastric emptying here is expressed in terms of the change in gastric liquid volume (V^L) , and the liquid volume in each 2D model corresponds to that in its equivalent 3D "surrogate" model.

S2D model, the A2D model shows a 56 % reduction in emptying rate, with 78 % of the liquid remaining after 10 min. This result demonstrates that even micron-level differences in pyloric dimensions can significantly affect emptying outcomes in 2D models. The dynamic mapping method developed in this study rigorously addresses the geometric differences between the 3D and 2D models, enabling the S2D model to capture subtle variations in pyloric opening (on the order of 1 \times 10 $^{-5}$ m) and ensure equivalent emptying behavior between 3D and 2D models.

Furthermore, the discrepancy between the A2D and 3D models highlights their differing flow loss characteristics: in the A2D model, the pyloric outlet forms a high-aspect-ratio slit ($l\gg d_4$), where the flow is dominated by slit-flow behavior, with increased aspect ratios leading to significantly greater flow losses (Raju and Kurian, 1995). This underscores the need to quantify flow characteristics using a discharge

coefficient. These comparisons highlight the significant influence of pyloric size and shape on gastric emptying rates in 2D models. The S2D model developed in this study employs a precise mapping approach to adjust the pyloric size, resulting in an emptying curve that closely matches that of the 3D model and aligns well with the gastric emptying curve observed in *in vivo* experiments (George, 1968) (see Fig. 11(c)), thereby validating its reliability. It should be noted that clinical gastric emptying reports typically use $t_{1/2}$ as a standard measure (Hellström et al., 2006). Therefore, this study focuses on the half-emptying process to align with clinical practices.

To further reveal the differences in flow characteristics among different models, we compared the instantaneous flow fields predicted by different models (3D, S2D, and C2D) at identical emptying stages (i. e., gastric retention at 95 %, 80 %, and 60 %). As shown in Fig. 12, due to

the rapid emptying rate ($t_{1/2} = 20$ s), the C2D model fails to capture even the first complete cycle of one ACW propagating from the corpus to the pylorus (60 s) (Harrison et al., 2018), which limits its ability to reflect the impact of ACWs on gastric flow dynamics. When discharging the same volume of liquid, the 3D and S2D models require nearly identical time, while the C2D model shows a much higher emptying rate. Notably, the C2D model's overestimated pyloric size results in predominantly unidirectional flow patterns, suppressing critical retrograde phenomena. In contrast, both the S2D and 3D models exhibit retropulsive flow near the pylorus, accompanied by recirculation eddies in the antral region, which is absent in the C2D model. The antral recirculation plays a critical role in the mixing and grinding of chyme under physiological conditions, and its accurate simulation is essential for understanding gastric motility.(Ferrua and Singh, 2010) This observation demonstrates that the S2D model can not only accurately predict the emptying rate, but also effectively reproduce the complex flow characteristics within the gastric cavity.

The expression for discharge coefficient (C_{d1}) in this study was successfully derived using only two 3D simulations with two fluids of different viscosities (F1: 0.001 Pa·s; F2: 0.01 Pa·s). In the following text, it will be demonstrated that the same expression is applicable to fluids with a variety of rheological properties. Further validations were carried out for fluids with different viscosities and densities (F3, F4, and F5) as well as common liquid foods (F6: orange juice, and F7: apple juice), whose physical properties are listed in Table 1.

It should be noted that the 3D simulations of F3 to F7 were carried out solely for generating ground truth data for S2D validation. One does not need these simulations to derive pyloric size in the S2D model. As shown in Fig. 13(a), to facilitate comparison, the variation of pyloric height (d_2) during gastric emptying is plotted on a logarithmic scale. The results indicate that d_2 gradually increases as emptying progresses for all cases. Low-viscosity fluids (F2, F6, F7) exhibited a faster rise in d_2 due to their higher emptying rates, while high-viscosity fluids (F3 to F5) showed a more gentle increase. Additionally, a trend of increasing average pyloric height was observed across all fluids as the emptying rate decreased. These findings confirm that the pyloric mapping approach dynamically adapts to variations in fluid properties, thereby ensuring the generality and predictive accuracy of the S2D model under diverse liquid conditions.

This generality can be further explained from a fluid mechanics perspective. According to Wu et al. (2002), the functional form of the discharge coefficient is primarily determined by the orifice geometry. In

 Table 1

 Rheological properties of fluids under investigation.

Fluids	ρ (kg/m ³)	μ (Pa•s)
F1 (Water)	1000	0.001
F2	1000	0.01
F3	1000	0.1
F4	1200	0.1
F5	1400	0.1
F6 (Orange juice (Islam et al., 2017))	1050	0.00625
F7 (Apple juice (Ortega-Rivas, 2012))	1044	0.025

our simulations, the pylorus maintains a circular cross-section throughout gastric emptying, with only its diameter varying over time. As a result, the geometric factor governing C_{d1} remains unchanged across different fluids. While variations in viscosity and density alter the Reynolds number, the empirical formulation for C_{d1} is valid over a broad range of Reynolds numbers. Moreover, the two fluids (F1 and F2) used for curve fitting already cover the range of Reynolds number under investigation, ensuring that the fitted expression is inherently applicable to other fluids without the need for additional fitting efforts.

Subsequently, the emptying curves predicted by the S2D model are compared with those by the 3D model (see Fig. 13(b)). Regardless of whether the fluids are the base-case fluids (water in Fig. 11(c)) or those with altered properties (F2 to F7), the S2D model maintains decent consistency with the 3D model, with a maximum deviation of approximately 8 % (for F5). Notably, both models captured the same trends in response to fluid property variations: low-viscosity fluids (F2, F6, F7) were emptied more rapidly, while high-viscosity fluids (F3-F5) demonstrated much slower emptying rates. Additionally, increased fluid density was associated with accelerated emptying (F3-F5). The capability of the S2D model to accurately replicate 3D results under diverse fluid conditions underscores its robustness and generality.

Furthermore, the S2D model demonstrates remarkable advantages in computational efficiency. As shown in Fig. 14, the solution time of the S2D model can be reduced by approximately 96 % as compared to the 3D model. Specifically, for gastric emptying simulation of water, the S2D model took only 3.7h, while the 3D model costed 108.2 h. Similarly, when simulating a higher-viscosity fluid (e.g., F3) with a slower emptying rate, the S2D model completed the simulation in 7.9 h, while the 3D model took up to 206 h. The computational efficiency advantage of S2D models enables researchers to complete about 25 groups of *in silico* stomach emptying experiments (by using the S2D models) within

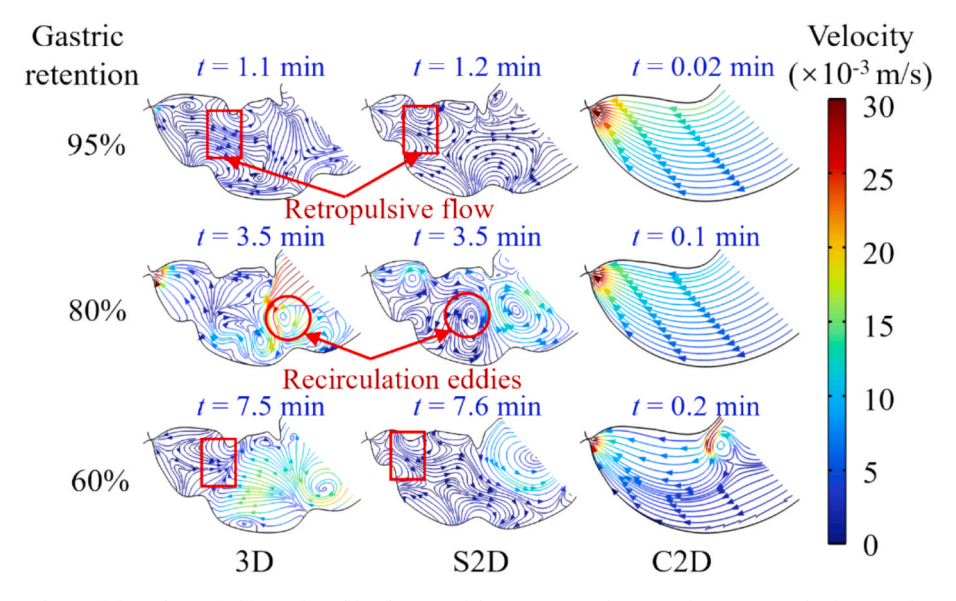


Fig. 12. Instantaneous streamlines of the velocity fields predicted by three models (3D, S2D and C2D), where rectangular boxes indicate retropulsive flows, while circular boxes highlight recirculation eddies.

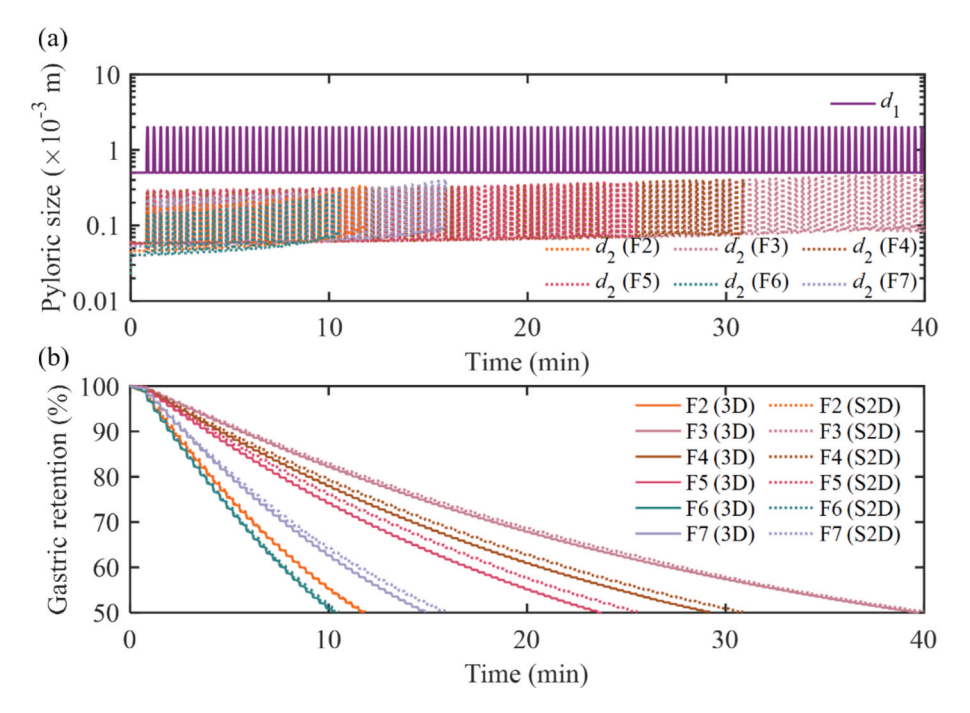


Fig. 13. Comparison of: (a) evolution of the logarithmic-scale pyloric size for different fluids in the 3D and surrogate 2D (S2D) models, and (b) gastric emptying curves for different fluids predicted by the two models. 3D model predictions serve as the ground truth.

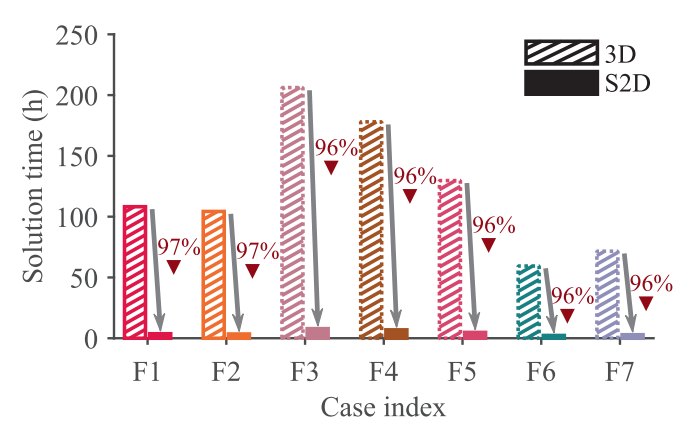


Fig. 14. Comparison of solution time between the S2D and 3D models for different cases. 3D simulations for F1 and F2 (shown with solid borders) are necessary for the derivation of pylorus size in the S2D model. However, 3D simulations for F3 to F7 (indicated with dashed borders) were carried out only for generating ground truth data that can be used to validate S2D model. All simulations were performed on a dual Intel Xeon Gold 5318Y CPU system, each with 24 cores running at 2.10 GHz.

the solution time that a single 3D simulation takes. This prominent advantage will greatly facilitate systematic and comprehensive multivariate (including various food properties and ACWs parameters) studies on stomach emptying behaviors. Comparative analyses confirm that changes in fluid viscosity and density have very slight influences on the computational efficiency of the S2D model, demonstrating the robustness on the efficiency of the method. Overall, the S2D CFD model proves to be highly effective and can serve as a valuable tool for quantitative evaluation of gastric emptying processes.

4. Conclusion

A surrogate 2D (S2D) CFD model was developed in this work to replace the 3D model for accurate prediction of gastric emptying with high computational efficiency. The key is the rigorous derivation of the

dynamic pylorus size in the S2D model based on in-depth understanding of geometric differences between S2D and 3D models. Specifically, the developed dynamic mapping approach can utilize only two sets of 3D gastric emptying simulation data for fluids with different viscosities to precisely adjust pyloric size in a S2D model, ensuring the consistency of emptying rates for both S2D and 3D models.

The S2D model overcomes the overestimation of emptying rates observed in the conventional 2D (C2D) model ($t_{1/2} = 20$ s), which directly uses the measured pyloric diameter as the pyloric height. The results indicate that the mapped pyloric height in the S2D model needs to be significantly smaller than the measured diameter, and the predicted half-emptying time ($t_{1/2}$) of the S2D model (10.2 min) closely matches that of the 3D model (9.8 min). Additionally, the S2D model demonstrates consistency with the 3D model in capturing complex gastric flow features, such as retropulsive flow and recirculation eddies, further validating its accuracy. By comparing the emptying processes of different fluids, including water, orange juice, apple juice, and other fluids with varying viscosities and densities, the S2D model exhibits broad generality with its emptying curves closely aligning with those of the 3D model. Moreover, the S2D model significantly improves computational efficiency, reducing simulation time by approximately 96 % compared to the 3D model. Although advances in computational power improve the feasibility of 3D simulations, the S2D model remains advantageous for extensive parametric studies and evaluations across diverse food properties, where numerous simulations are required. Moreover, with improved computational efficiency, much longer emptying time can be simulated, which will be important to understand the emptying behavior of food systems with low emptying rates.

In summary, the S2D model developed for stomach emptying ensures computational accuracy, significantly enhances computational efficiency and demonstrates generality to fluids with diverse rheological properties. This model offers an efficient and reliable tool for predicting gastric emptying, possessing substantial theoretical value and practical application potentials.

CRediT authorship contribution statement

Xin Zhang: Writing - review & editing, Writing - original draft,

Visualization, Validation, Software, Methodology, Investigation, Formal analysis. Xianchen Huang: Writing – review & editing, Formal analysis. Xiao Dong Chen: Writing – review & editing, Supervision, Formal analysis. Jie Xiao: Writing – review & editing, Visualization, Validation, Supervision, Resources, Project administration, Methodology, Funding acquisition, Formal analysis, Conceptualization.

Declaration of competing interest

The authors declare that they have no known competing financial interests or personal relationships that could have appeared to influence the work reported in this paper.

Acknowledgements

We are grateful for the financial support from the National Natural Science Foundation of China (21978184), the "Jiangsu Innovation and Entrepreneurship (Shuang Chuang) Program", the "Jiangsu Specially Appointed Professors Program", and the "Priority Academic Program Development (PAPD) of Jiangsu Higher Education Institutions".

Appendix A. Supplementary data

Supplementary data to this article can be found online at https://doi.org/10.1016/j.ces.2025.122558.

Data availability

The simulation data corresponding to Figures 6-9, 11, 13, and 14 are available in the Supplementary Data S1.

References

- Alajmi, A., Ali, S.S., Alkhudhari, M., Alqaffas, J., Carrasco, Z., Payan, J., Pasamba, M., Zirakian, T., Boyajian, D., 2019. A civil engineering senior design research effort to ascertain discharge coefficients of different orifice geometries. J. Civ. Eng. Archit. 13, 204–208. https://doi.org/10.17265/1934-7359/2019.03.005.
- Csendes, A., Burgos, A.M., 2005. Size, volume and weight of the stomach in patients with morbid obesity compared to controls. Obes. Surg. 15, 1133–1136. https://doi.org/ 10.1381/0960892055002158.
- Ebara, R., Ishida, S., Miyagawa, T., Imai, Y., 2023. Effects of peristaltic amplitude and frequency on gastric emptying and mixing: a simulation study. J. R. Soc. Interface 20, 20220780. https://doi.org/10.1098/rsif.2022.0780.
- Eyre-Brook, I.A., Smallwood, R.H., Linhardt, G.E., Johnson, A.G., 1983. Timing of pyloric closure in man: studies with impedance electrodes. Digest Dis Sci 28, 1106–1115. https://doi.org/10.1007/BF01295810.
- Ferrua, M.J., Singh, R.P., 2010. Modeling the fluid dynamics in a human stomach to gain insight of food digestion. J. Food Sci. 75, 151–162. https://doi.org/10.1111/j.1750-3841_2010_01748_x
- George, J.D., 1968. New clinical method for measuring the rate of gastric emptying: the double sampling test meal. Gut 9, 237–242. https://doi.org/10.1136/gut.9.2.237.
- Hao, S.L., Wang, B., Wang, Y., 2015. Density-dependent gastroretentive microparticles motion in human gastric emptying studied using computer simulation. Eur. J. Pharm. Sci. 70, 72–81. https://doi.org/10.1016/j.ejps.2015.01.009.
- Harrison, S.M., Cleary, P.W., Sinnott, M.D., 2018. Investigating mixing and emptying for aqueous liquid content from the stomach using a coupled biomechanical-SPH model. Food Funct. 9, 3202–3219. https://doi.org/10.1039/C7F001226H.
- Hellström, P.M., Grybäck, P., Jacobsson, H., 2006. The physiology of gastric emptying. Best Pract. Res. Clin. Anaesthesiol. 20, 397–407. https://doi.org/10.1016/j. bpa.2006.02.002.

- Ishida, S., Miyagawa, T., O'Grady, G., Cheng, L.K., Imai, Y., 2019. Quantification of gastric emptying caused by impaired coordination of pyloric closure with antral contraction: a simulation study. J. R. Soc. Interface 16, 20190266. https://doi.org/ 10.1098/rsif.2019.0266.
- Islam, M.Z., Kitamura, Y., Kokawa, M., Monalisa, K., Tsai, F.-H., Miyamura, S., 2017. Effects of micro wet milling and vacuum spray drying on the physicochemical and antioxidant properties of orange (Citrus unshiu) juice with pulp powder. Food Bioprod. Process. 101, 132–144. https://doi.org/10.1016/j.fbp.2016.11.002.
- Kamaltdinov, M., Trusov, P.V., Zaitseva, N.V., 2024. Investigation of digestion processes in the stomach and duodenum using computational fluid dynamics model. CFD Lett. 16, 82–95. https://doi.org/10.37934/cfdl.16.3.8295.
- Kozu, H., Kobayashi, I., Nakajima, M., Uemura, K., Sato, S., Ichikawa, S., 2010. Analysis of flow phenomena in gastric contents induced by human gastric peristalsis using CFD. Food Biophys. 5, 330–336. https://doi.org/10.1007/s11483-010-9183-y.
- Kuhar, S., Lee, J.H., Seo, J.-H., Pasricha, P.J., Mittal, R., 2022. Effect of stomach motility on food hydrolysis and gastric emptying: insight from computational models. Phys. Fluids 34, 111909. https://doi.org/10.1063/5.0120933.
- Kuhar, S., Seo, J.-H., Pasricha, P.J., Mittal, R., 2024. In silico modelling of the effect of pyloric intervention procedures on gastric flow and emptying in a stomach with gastroparesis. J. R. Soc. Interface 21, 20230567. https://doi.org/10.1098/ rsif.2023.0567.
- Lee, J.H., Kuhar, S., Seo, J.-H., Pasricha, P.J., Mittal, R., 2022. Computational modeling of drug dissolution in the human stomach: effects of posture and gastroparesis on drug bioavailability. Phys. Fluids 34, 081904. https://doi.org/10.1063/5.0096877.
- Li, C., Chen, X.D., Xiao, J., Deng, R., Jin, Y., 2024. Impact of reduced gravity on food mixing and emptying in human stomach: a numerical simulation study. Phys. Fluids 36, 061908. https://doi.org/10.1063/5.0208898.
- Li, C., Xiao, J., Chen, X.D., Jin, Y., 2021. Mixing and emptying of gastric contents in human-stomach: a numerical study. J. Biomech. 118, 110293. https://doi.org/ 10.1016/j.jbiomech.2021.110293.
- Liu, X., Fletcher, D.F., Bornhorst, G.M., 2024. A review of the use of numerical analysis in stomach modeling. J. Food Sci. 89, 3894–3916. https://doi.org/10.1111/1750-3841.17157
- Marciani, L., Gowland, P.A., Moore, R.J., Young, P., Al-Sahab, S., Spiller, R.C., Manoj, P., Bush, D., Wright, J., Fillery-Travis, A.J., 2000. Gastric response to increased meal viscosity assessed by echo-planar magnetic resonance imaging in humans. J. Nutr. 130, 122–127. https://doi.org/10.1093/in/130.1.122.
- Maurer, A.H., 2012. Advancing gastric emptying studies: standardization and new parameters to assess gastric motility and function. Semin. Nucl. Med. 42, 101–112. https://doi.org/10.1053/j.semnuclmed.2011.10.001.
- Ortega-Rivas, E., 2012. Non-thermal Food Engineering Operations. Food Engineering Series. Springer. New York.
- Pal, A., Brasseur, J.G., Abrahamsson, B., 2007. A stomach road or "Magenstrasse" for gastric emptying. J. Biomech. 40, 1202–1210. https://doi.org/10.1016/j. ibiomech.2006.06.006.
- Pal, A., Indireshkumar, K., Schwizer, W., Abrahamsson, B., Fried, M., Brasseur, J.G., 2004. Gastric flow and mixing studied using computer simulation. Proc. R. Soc. Lond. B 271, 2587–2594. https://doi.org/10.1098/rspb.2004.2886.
- Phillips, L.K., Deane, A.M., Jones, K.L., Rayner, C.K., Horowitz, M., 2015. Gastric emptying and glycaemia in health and diabetes mellitus. Nat. Rev. Endocrinol. 11, 112–128. https://doi.org/10.1038/nrendo.2014.202.
- Raju, C., Kurian, J., 1995. Effect of slit aspect ratio on free jet properties. Vacuum 46, 389–395. https://doi.org/10.1016/0042-207X(94)00085-9.
- Toniolo, I., Berardo, A., Gagner, M., Foletto, M., Carniel, E.L., 2023. Unveiling the effects of key factors in enhancing gastroesophageal reflux: a fluid-structure analysis before and after laparoscopic sleeve gastrectomy. Comput Meth Prog Bio. 231, 107409. https://doi.org/10.1016/j.cmpb.2023.107409.
- Trusov, P.V., Zaitseva, N.V., Kamaltdinov, R., 2013. Simulation of digestion processes in consideration of functional disorders in a human organism: conceptual and mathematical formulations, model structure. Russ. J. Biomech. 17, 60–74.
- Wu, D., Burton, R., Schoenau, G., 2002. An empirical discharge coefficient model for orifice flow. Int. J. Fluid Power 3, 13–19. https://doi.org/10.1080/ 14399776.2002.10781143
- Xu, F., Zhang, H., Fan, Z., Zheng, Z., Sun, A., Zhang, J., 2024. Investigating biomechanical alterations and emptying patterns after various gastrojejunostomy strategy. Food Res. Int. 176, 113815. https://doi.org/10.1016/j. foodres 2023 113815